Applied Mechanics and Materials Vol. 566 (2014) pp 563-568

doi:10.4028/www.scientific.net/AMM.566.563

Dynamic Crushing of Voronoi Honeycombs: Local Stress-strain States

Jilin Yu[1,a], Shenfei Liao[1,b], Zhijun Zheng[1,c] and Changfeng Wang[1,d]

[1]CAS Key Laboratory of Mechanical Behavior and Design of Materials, University of Science and Technology of China, Hefei, Anhui 230026, PR China

[a]jlyu@ustc.edu.cn, [b]liao1985@mail.ustc.edu.cn, [c]zjzheng@ustc.edu.cn, [d]wcfgclx@mail.ustc.edu.cn

Keywords: Dynamic crushing; Voronoi honeycomb; Strain field; Stress-strain state.

Abstract: Dynamic stress-strain states in Voronoi honeycombs are investigated by using cell-based finite element models. Two different loading scenarios are considered: the high-constant-velocity compression and the direct impact. The 2D local engineering strain fields are calculated. According to the feature of shock front propagation, the 1D distribution of local engineering strain in the loading direction is deduced from the 2D strain fields, which provide evidences of the existence of discontinuities at shock front in cellular materials and thus enhance the basis of the continuum-based shock models. A method to quantitatively clarify the local stress-strain states ahead of and behind the shock front is developed. The results show that the dynamic stress-strain states in the densification stage obtained from both loading scenarios are different from the quasi-static stress-strain relation. The stress ahead of the shock front obtained from the high-constant-velocity compression scenario is slightly smaller than the quasi-static yield stress, but that obtained from the direct impact scenario is larger than the quasi-static yield stress. The possible mechanisms of deformation and wave propagation are explored.

Introduction

Nominal stress-strain curves are commonly used to represent the constitutive behaviour of materials. However, this is not appropriate for cellular metals when subjected to high-velocity impact/compression, because their deformation is localized and the stresses at the two ends of a specimen are very different [1-3]. To represent the dynamic constitutive behaviour of cellular metals, it is needed to define and measure the 'local' strain.

Several methods have been developed to calculate the 'local' strain. Zou et al. [4] presented a definition of local engineering strain for regular honeycombs based on the relative displacement between two neighboring cross-sections. However, this method is more suitable for high-velocity impact than for low-velocity impact because the definition of local strain masked the gross behavior over the transverse direction. Moreover, the strain behind the shock front suffers high fluctuations and thus is difficult for quantitative analysis. Mangipudi and Onck [5] proposed a local strain map algorithm for Voronoi honeycombs by triangulating Voronoi cells into triangles, but the local strain in this approach was defined by Cauchy strain formula and thus is only appropriate for small-strain states. Most recently, Liao et al. [6, 7] developed a strain field calculation method based on the optimal local deformation gradient technique to quantitatively characterize the deformation and strain localization for cellular materials. The strain field calculation method allows considering general finite-strain states of both regular and irregular cellular materials.

In this paper, the strain field calculation method is employed to investigate the dynamic stress-strain states in cellular materials using a 2D cell-based finite element model. Different loading scenarios with different compression/impact velocities are considered.

Numerical models

Voronoi honeycombs, constructed by 2D random Voronoi technique [8] with cell irregularity of 0.5, are used to model cellular metals in this study, as illustrated in Fig. 1. The specimen of Voronoi honeycomb is generated in an area of 400×100 mm^2 with 1600 nuclei. The relative density of the specimen is taken to be $\rho_0/\rho_s = 0.1$, where ρ_0 is the initial density of the Voronoi honeycomb and ρ_s the density of the cell-wall material. Two typical loading scenarios, as illustrated in Fig. 1, are considered in this study. One is the constant-velocity compression, i.e. a rigid surface with a constant velocity V strikes the stationary Voronoi honeycomb rod supported by another rigid surface. The other is the direct impact, i.e. the Voronoi honeycomb rod with an initial velocity V_0 directly strikes at a rigid stationary target.

The finite element code ABAQUS/Explicit is employed to perform the numerical simulations. The cell-wall material is assumed to be elastic, perfectly plastic with Young's modulus E = 69 GPa, yield stress Y = 170 MPa, density ρ_s = 2770 kg/m^3 and Poisson's ratio ν = 0.3. The cell walls of Voronoi honeycombs are modeled with S4R (a 4-node doubly curved, reduced integration) shell elements, of which the size was set to be about 0.6 mm in-plane and 1 mm out-of-plane through a mesh sensitivity analysis. All possible contacts are considered by defining general contact with slight friction as used in [8]. To simulate an in-plane strain state, all the nodes are constrained in the out-of-plane direction.

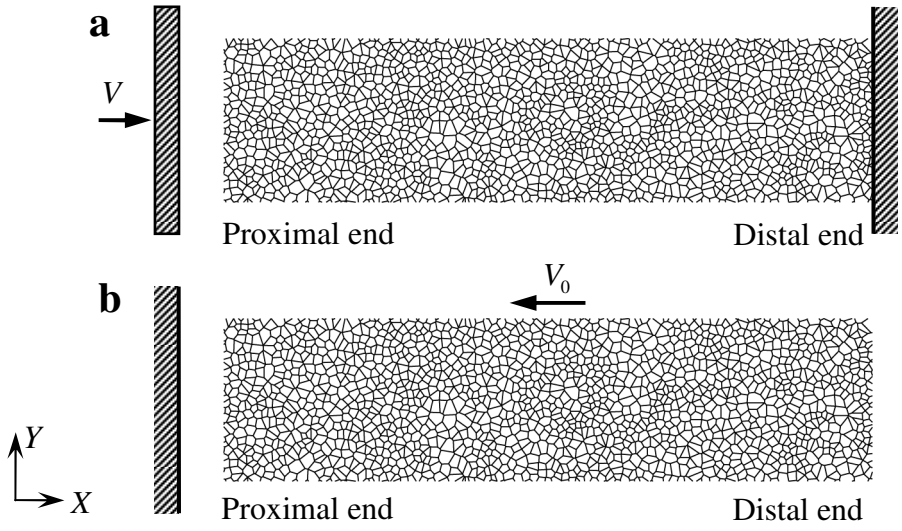

Fig. 1. Finite element models of Voronoi honeycombs:
(a) under the constant-velocity compression and (b) under the direct impact.

Deformation patterns and strain fields

Deformation patterns for Voronoi honeycombs under loadings are shown in Figs. 2 and 3. The deformation is localized close to the proximal end of the specimen for both loading scenarios. Cells collapse layer-by-layer and a deformation front propagates from the proximal end to the distal end.

To characterize the deformation features, the strain field calculation method developed by Liao et al. [7] is employed to calculate the local strain in the X-direction. This method is briefly described here. Two nodal configurations, namely the reference (undeformed) configuration Ω_0 and the current (deformed) configuration Ω_1, are needed to calculated the local deformation gradient. For node i and its neighboring node j, their relative position vectors are $\mathbf{U}_{ij} = \mathbf{X}_j - \mathbf{X}_i$ and $\mathbf{u}_{ij} = \mathbf{x}_j - \mathbf{x}_i$ in configurations Ω_0 and Ω_1, respectively, where $\mathbf{X}$ and $\mathbf{x}$ are the position vectors of a node in Ω_0 and Ω_1, respectively. All these vectors are considered in *column*. For node i, its optimal local deformation gradient can be calculated by

$$\mathbf{F}_i = \mathbf{W}_i \cdot \mathbf{V}_i^{-1}, \tag{1}$$

with matrixes $\mathbf{V}_i = \sum_{j \in N_c} \mathbf{U}_{ij} \cdot \mathbf{U}_{ij}^{\mathrm{T}}$ and $\mathbf{W}_i = \sum_{j \in N_c} \mathbf{u}_{ij} \cdot \mathbf{U}_{ij}^{\mathrm{T}}$, where N_c is the set of neighboring nodes of node i with a cut-off radius R_c as discussed in [7], and superscript T denotes the transpose of a matrix. Large deformation can then be represented by the Lagrangian/Green strain tensor

$$\mathbf{E}_i = \frac{1}{2}\left(\mathbf{F}_i^{\mathrm{T}} \cdot \mathbf{F}_i - \mathbf{I}\right), \tag{2}$$

where $\mathbf{I}$ is the identity matrix. A numerical scheme performing scattered data interpolation based on an underlying Delaunay triangulation is used to achieve continuous strain field from the data of discrete strains.

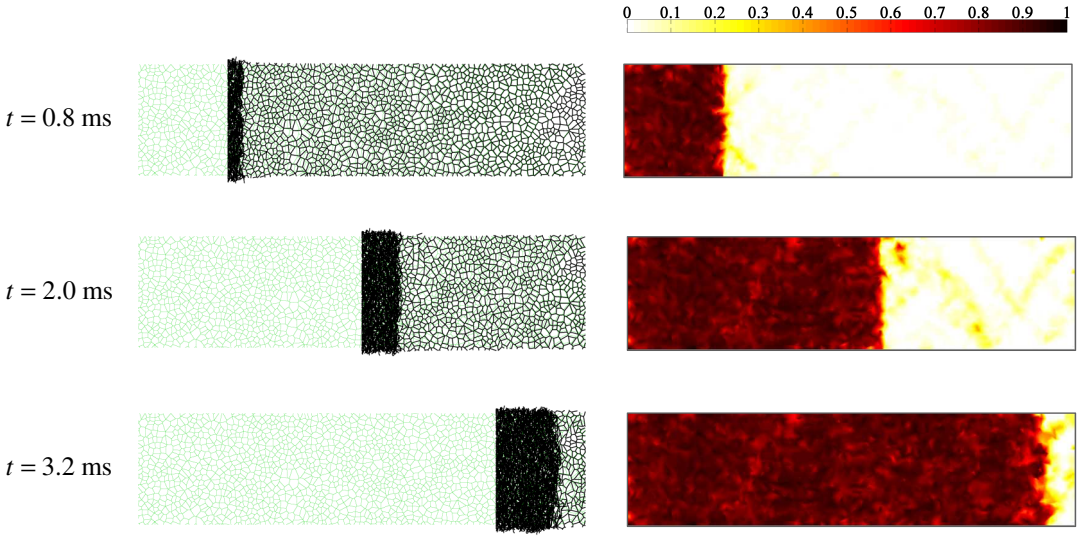

Fig. 2. Deformation patterns (left) and their corresponding local strain fields (right) for the Voronoi honeycomb under constant-velocity compression with V = 100 m/s.

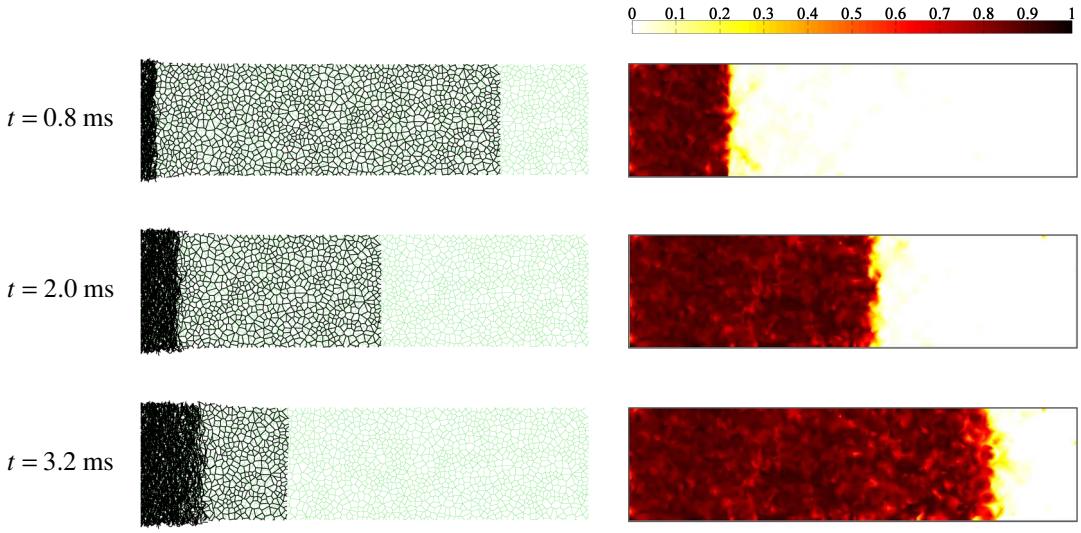

Fig. 3. Deformation patterns (left) and their corresponding local strain fields (right) for the Voronoi honeycomb under direct impact with V_0 = 100 m/s.

The 2D fields of local engineering strain in the *X*-direction are also shown in Fig. 2 and 3. In each loading scenario, there exists an apparent discontinuity that separates the region of large plastic strain near the proximal end and the region of low strain near the distal end. The discontinuity propagates through the Voronoi honeycomb from the proximal end to the distal end as the impact continues. Thus, the local strain fields clearly capture the shock front propagation in the Voronoi honeycombs.

Strain distributions

According to the feature of shock front propagation, the 1D distributions of local engineering strain in the loading direction are deduced from the 2D strain fields as done in Ref. [6]. Fig. 4 shows the 1D strain distributions, which provide evidences of the existence of discontinuities at shock front in cellular materials. Thus, these results based on cell-based finite element models enhance the basis of the continuum-based shock models.

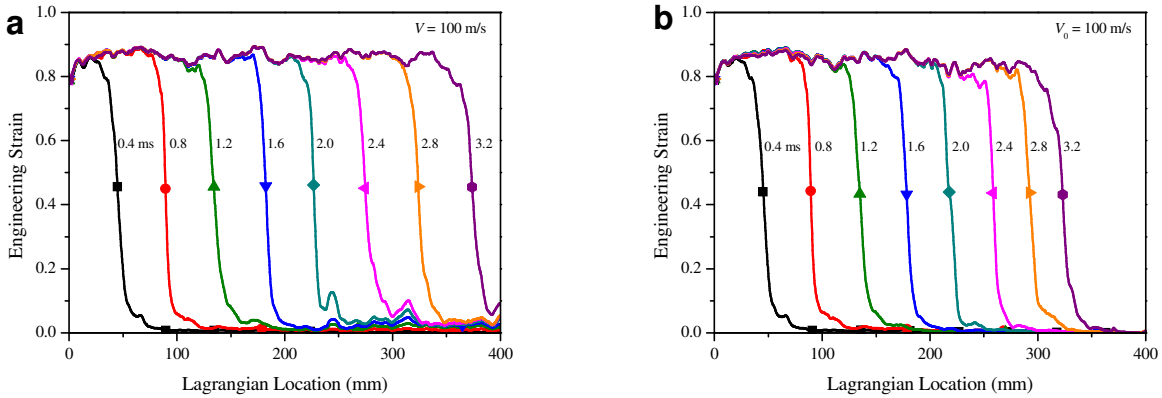

Fig. 4. Local strain distributions of Voronoi honeycombs:
(a) under the constant-velocity compression and (b) under the direct impact.

Stress-strain states

Measuring the local strain in cellular materials, which is much difficult in experiments, is achieved in the numerical 'test' by the strain field calculation method. Therefore, it provides an essential method to quantitatively clarify the dynamic stress-strain states in cellular materials.

For the constant-velocity compression scenario, the stresses ahead of and behind the shock front are taken as the plateau stresses at the distal end and the proximal end, respectively, and calculated as in [6]. The strain behind the shock front is calculated by averaging the local strain over the compacted region. For the direct impact scenario, the stress at the proximal end shows large oscillation, as shown in Fig. 5a which displays the time history of the stress at V_0 = 100 m/s. The strain behind the shock front, calculated as in [9], is also shows data oscillation, as shown in Fig. 5b. In order to ignore the influence of the data oscillation, the time history of the stress at the proximal end and the strain behind the shock front are both fitted by using

$$f = (\alpha_1 + \alpha_2 t)/(1+\alpha_3 t), \tag{3}$$

where f is dependent variable, t is independent variable, i.e. impact time, and α_1, α_2, α_3 are coefficients. The fitted results are also shown in Fig. 5. The stress ahead of the shock front σ_A can be obtained by the Rankine-Hugoniot relations across the shock front as

$$\sigma_A(t) = \sigma_B(t) - \frac{\rho_0 v^2(t)}{\varepsilon_B(t)}, \tag{4}$$

where σ_B is the stress behind the shock front, ε_B the strain behind the shock front, ρ_0 the initial density of the Voronoi honeycomb, and v the impact velocity.

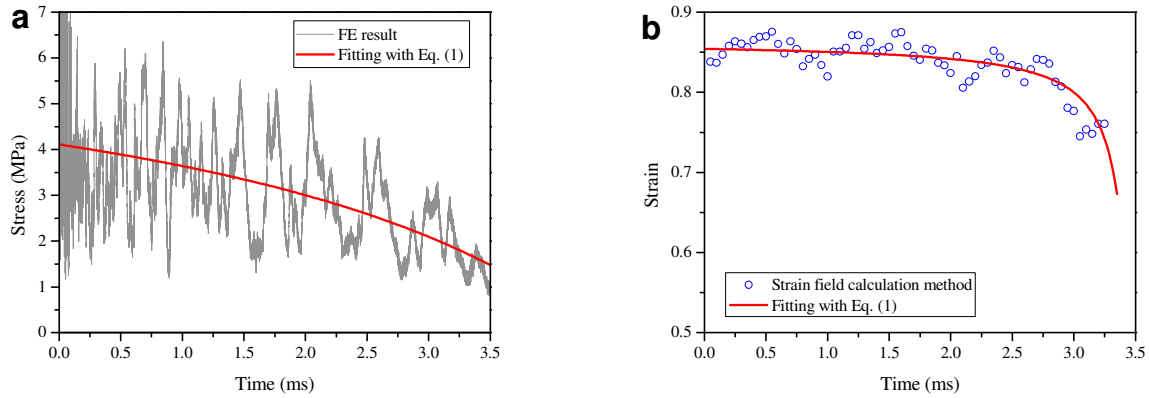

Fig. 5. (a) The stress at the proximal end and (b) the strain behind the shock front for the direct impact scenario.

The stresses ahead of the shock front for the two loading scenarios at different impact velocities are shown in Fig. 6a. It is demonstrated that the stress ahead of the shock front obtained from the constant-velocity compression scenario is smaller than the quasi-static yield stress, but that obtained from the direct impact scenario is larger than the quasi-static yield stress.

The stress-strain states behind the shock front for the two loading scenarios at different impact velocities are shown in Fig. 6b, similarly as the phenomenon found in a 3D Voronoi structure [9]. It transpires that the dynamic stress-strain states in the densification stage are different from the quasi-static stress-strain relation.

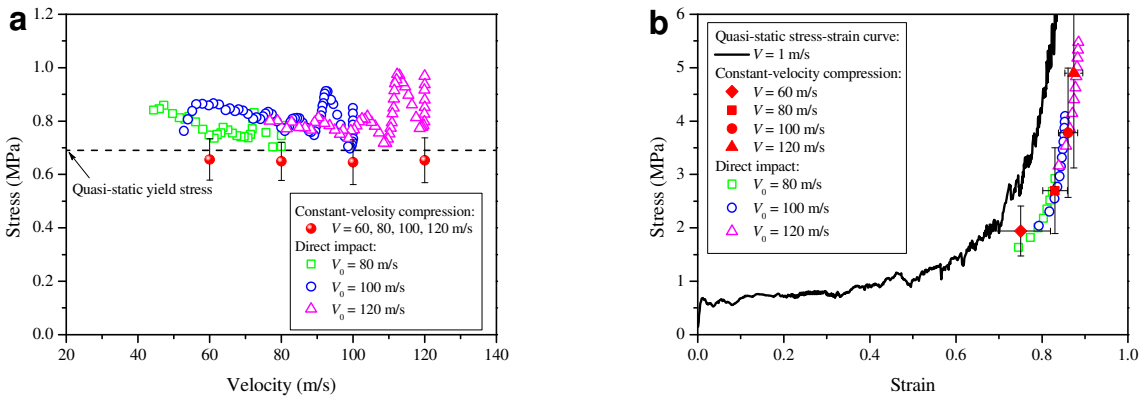

Fig. 6. (a) The stress ahead of the shock front versus the impact velocity; (b) The stress-strain relations for the constant-velocity compression and the direct impact scenarios.

Under quasi-static compression, the deformation occurs as shear bands which are randomly distributed in the Voronoi honeycomb, as shown in Fig. 7. This indicates that a Voronoi honeycomb deformed with shear bands needs less energy than that collapsed in a layer-wise manner under the direct impact scenario shown in Fig. 3. In fact, the stress ahead of the shock front in the specimen under direct impact always corresponds to the dynamic initial crush stress, but that in the specimen under constant-velocity compression only corresponds to the initial crush stress at a particular time and after this time its value reduces.

The randomly distributed shear bands under quasi-static compression may meet and interact with each other as the overall compression continues, as shown in Fig. 7. Such interaction leads to an increase of compression resistance. This deformation feature explains the slight plastic strain-hardening characteristic of the quasi-static nominal stress-strain curve. However, under high-velocity compression/impact, cells collapse in a layer-wise manner at a relatively stable stress level and the interaction between the collapsed layers is very weak. Therefore, high loading rate leads to a more compact deformed pattern with a larger densification strain. This discrepancy of deformation feature is believed to make the dynamic stress-strain states different from the quasi-static nominal stress-strain relation in the densification stage, as shown in Fig. 6b.

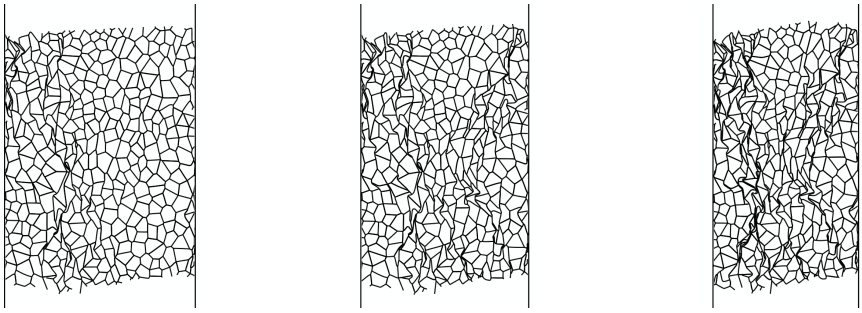

Nominal strain: 0.2 Nominal strain: 0.3 Nominal strain: 0.4

Fig. 7. Deformation patterns of a Voronoi honeycomb under quasi-static compression (V = 1 m/s).

Summary

Dynamic local stress-strain states in Voronoi honeycombs are investigated by using cell-based finite element models. The 2D fields and 1D distributions of local engineering strain in the loading direction of Voronoi honeycombs under two different loading scenarios are obtained by the strain field calculation method. These results provide evidences of the existence of discontinuities at shock front in cellular materials and thus enhance the basis of the continuum-based shock models. The stress ahead of the shock front obtained from the constant-velocity compression scenario is smaller than the quasi-static yield stress, while that obtained from the direct impact scenario is larger than the quasi-static yield stress. The dynamic stress-strain states obtained from both impact scenarios are different from the quasi-static stress-strain relation. Finally, the possible mechanisms of deformation and wave propagation are explored.

Acknowledgements

This work is supported by the National Natural Science Foundation of China (Projects Nos. 11002140, 90916026 and 10932011).

References

[1] Tan PJ, Reid SR, Harrigan JJ, Zou Z, Li S: J. Mech. Phys. Solids Vol. 53 (2005), p. 2174.
[2] Liu YD, Yu JL, Zheng ZJ, Li JR: Int. J. Solids Struct. Vol. 46 (2009), p. 3988.
[3] Tan PJ, Reid SR, Harrigan JJ: Int. J. Solids Struct. Vol. 49 (2012), p. 2744.
[4] Zou Z, Reid SR, Tan PJ, Li S, Harrigan JJ: Int. J. Impact Eng. Vol. 36 (2009), p.165.
[5] Mangipudi KR, Onck PR: J. Mech. Phys. Solids Vol. 59 (2011), p. 1437.
[6] Liao SF, Zheng ZJ, Yu JL: Int. J. Impact Eng. Vol. 57 (2013), p. 7.
[7] Liao SF, Zheng ZJ, Yu JL: Int. J. Solids Struct. Vol.51 (2014), p.478.
[8] Zheng ZJ, Yu JL, Li JR: Int. J. Impact Eng. Vol. 32 (2005), p. 650.
[9] Wang CF, Zheng ZJ, Yu JL, Reid SR, Harrigan JJ: submitted to J. Mech. Phys. Solids (2013).